

# Dust envelope modelling of the Red Rectangle nebula

Bruno Lopez<sup>1</sup>, Eric Tessier<sup>2</sup>, Pierre Cruzalèbes<sup>3</sup>, Jean Lefèvre<sup>1</sup>, and Thibaut Le Bertre<sup>4</sup>

<sup>1</sup> Observatoire de la Côte d'Azur, Département Fresnel UMR 6528, BP 4229, F-06034 Nice Cedex 4, France

<sup>2</sup> Groupe d'Astrophysique, Observatoire de Grenoble, Université Joseph-Fourier, BP 53X, F-38041 Grenoble Cedex, France

<sup>3</sup> Observatoire de la Côte d'Azur, Département Fresnel UMR 6528, Av. Copernic, F-06130 Grasse, France

<sup>4</sup> DEMIRM, Observatoire de Paris, 61 av. de l'Observatoire, F-75014 Paris, France

Received 9 July 1996 / Accepted 5 December 1996

**Abstract.** Radiative transfer modelling of the dust shell of the post-AGB Red Rectangle nebula is proposed in non-spherical geometry. The present work follows a previous study by Yusef-Zadeh et al. (1984) in which the dust density law smoothly decreases with latitude above and below the midplane of the disc shaped envelope.

Our aim is to take account of new observational constraints in addition to those already imposed by the image of the nebula at visible wavelengths. The broad band spectrum is fitted. The infrared map at  $2.2\mu\text{m}$  is also taken into account for our model. As a result of our study, we find that the best compromise in the choice of the model parameters leads to a dust density law which differs from the one proposed previously. The temperature of the hottest grains is about 1000 K. Large dust particles are present in the circumstellar environment, the largest of these being probably confined to the plane of the disc.

We estimate the dust shell mass to be about  $3.8 \times 10^{-4}M_{\odot}$  assuming a distance of 330 pc for the Red Rectangle (Cohen et al. 1975).

**Key words:** radiative transfer – stars: individual: HD 44179 – circumstellar matter

---

## 1. Introduction

### 1.1. General aspects of the Red Rectangle

HD 44179 is a ninth magnitude star at visible wavelengths, embedded in a nebulosity of remarkable symmetry. A wide range of observational techniques has been employed by Cohen et al. (1975) to suggest a descriptive model of the source. HD 44179 consists of one or two stars of spectral type B9-A0 III. The star and its associated nebula have been called the Red Rectangle because of the appearance in the red continuum of a rectangular shape with four prominent bright diagonal spikes (also existing

in the yellow). The brightness of these spikes is enhanced in polarized light both in the red and in the blue (Perkins et al. 1981). This peculiar geometry results from a disk of gas and dust which surrounds HD 44179, the line of sight lying close to the plane of the disk. The presence of circumstellar dust is suggested by:

- the excess of infrared radiation
- the polarimetric measurements
- some infrared spectral features.

The Red Rectangle is known to be a post-AGB star. CO has been found in absorption in the UV spectrum (Sitko 1983) as well as in radio emission (Jura et al. 1995). This circumstellar molecular emission and the lack of connection with any interstellar cloud have led Bachiller et al. (1986) to consider the Red Rectangle as an evolved star.

The environment of the Red Rectangle is carbon rich (Bregman et al. 1993). Several chemical materials have been proposed to explain the set of unidentified infrared emission features centered at 3.3, 6.2, 7.7, 8.6 and  $11.3\mu\text{m}$  (Allamandola 1989): polycyclic aromatic hydrocarbon (PAH) (Léger and Puget 1984); hydrogenated amorphous carbon (HAC) (Duley and Williams 1981); quenched carbonaceous composite (QCC) (Sakata et al. 1984). Although carbon enters into the composition of all of these materials, it is not clear that the central star HD 44179 possesses a carbon-rich photosphere as expected. The abundances of photospheric elements C, N, O, S are almost solar-like while the abundances of Fe, Mg, Ca and Si are extremely low (Waelkens et al. 1992). The presence of dust may explain the depletion of heavier elements in the photospheric gas (Mathis and Lamers 1992, and Waters et al. 1992).

A peculiar molecular emission (Schmidt et al. 1980) which seems to originate in the surrounding nebula has been detected in red light. Low resolution optical spectrophotometry measurements of the reflexion nebula do reveal an important broad bump from about  $0.57$  to  $0.70\mu\text{m}$  (called extended red emission, ERE) containing five unidentified sharp emission features near  $0.58\mu\text{m}$ . The ERE could be produced by the photoluminescence of HAC grains (Duley 1985) while the emission features could

---

*Send offprint requests to:* Bruno Lopez

be related to a molecular emission (Schmidt and Witt 1991). A re-examination of the spectra of the nebulosity in the Red Rectangle shows that the wavelengths of the four most prominent emission bands correspond closely with one of the proposed families of diffuse interstellar absorption bands (Scarrott et al. 1992).

### 1.2. Our goal

Morris (1981) has shown that the dusty envelope constituting an axisymmetric nebula may be represented by a dust density law smoothly decreasing with latitude above (and below) the midplane. In this model, the radial extension of the envelope is identical at all latitudes. Alternatively, Icke (1981) assumed that the radial extension of a nebula might depend on the latitude angle. For example, a small and optically thick torus of dust may exist around HD 44179 and may be responsible for the appearance of the nebula.

The geometrical model proposed by Morris (1981) has been successfully exploited by Yusef-Zadeh et al. (1984) who studied the latitude distribution of dust particles for the Red Rectangle and two other objects (CRL 2688 and M1-92). The albedo, the phase function of the particles and the optical depth of the envelope were the sensitive parameters analyzed by Yusef-Zadeh et al. (1984). The following results were obtained:

- confirmation of the interest of the Morris's model for the Red Rectangle (i.e. radial extension of the envelope equal at all latitude angles)
- estimation of a dust distribution latitude law
- role of dust multiple scattering to explain the shape observed at visible wavelengths.

In our study we have extended the Yusef-Zadeh et al. (1984) investigation to build a model of the Red Rectangle coherent with a wider range of observational data. The radiative transfer simulation that has been used computes the radiative transfer as well as the radiative equilibrium for dust grains. This additional step in the simulation allows the calculation of the dust temperature anywhere in the envelope. The spectral energy distribution of the object can then be modeled as well as any infrared image in which dust thermal radiations exist. A wider range of physical parameters can be studied.

In Sect. 2 we present a compilation of infrared images obtained by means of high angular resolution imaging. Some speckle interferometric observations (Cruzalèbes et al. 1996) and a large set of adaptive optics observations (Rouan 1993, Tessier et al. 1990, Roddier et al. 1995) provide, in the near infrared and at spatial resolution ranging from 0.2 to 0.3 arcsec, a new insight on the circumstellar environment.

Additional observational constraints used for the modelling are presented in Sect. 3. Some details of the simulation employed as well as the different assumptions used are described in Sect. 4. In Sect. 5, different Red Rectangle models are presented. Their interests are discussed together. The validity range of the modelling and the accuracy of the parameters determination are considered.

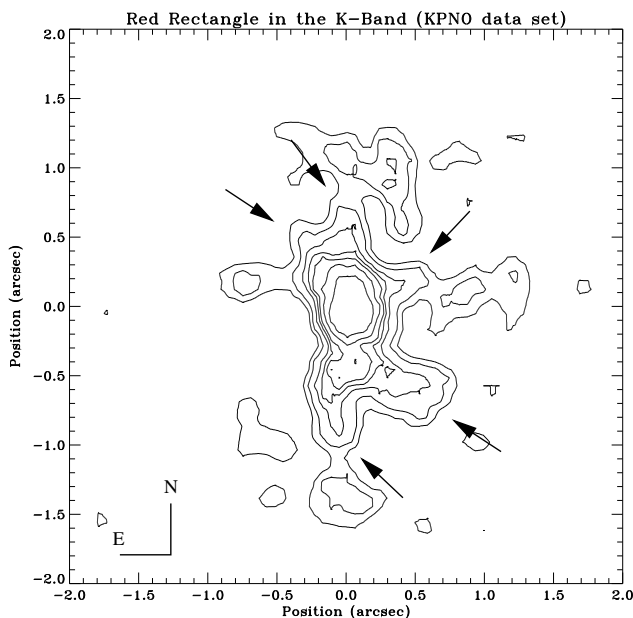


**Fig. 1.** The  $2.2\mu\text{m}$  image of the Red Rectangle nebula obtained with the 3.8 m telescope of Kitt Peak Observatory (Cruzalèbes et al. 1995). The arrows show the structures common to all infrared images. Overplotted contours are 0.5, 1, 2, 3, 5, 10 and 20% of the maximum of intensity. Lowest contour is three times the standard deviation of the noise, measured in regions external to the nebula.

## 2. Appearance of the Red Rectangle in the infrared

Many observations of the Red Rectangle have been carried out at high angular resolution (HRA). Some low light level structures in the Red Rectangle images obtained with different near infrared techniques are common and may be attributed to real structures in the nebula.

We have compared adaptive optics images obtained by the Come-On+ experiment in May 91 at the ESO 3.6-m telescope (La Silla) in the spectral bands J ( $1.25\mu\text{m}$ ), H ( $1.65\mu\text{m}$ ), K ( $2.2\mu\text{m}$ ), L ( $3.8\mu\text{m}$ ) and M ( $4.8\mu\text{m}$ ) (Rouan 1993), with speckle reconstructed images from the CFHT 3.6-m telescope (Hawāi) in December 90 in L' ( $3.87\mu\text{m}$ ) and M, and from the KPNO 3.8-m telescope (Kitt Peak) in November 87 in K band (Cruzalèbes et al. 1996, see Fig. 1). The overlap of the structures contained in the different set of images is a criterium of reliability. Another criterium of reliability is the size of the structure which has to be equal to or greater than the angular resolution (given by the full width at half maximum of the point-spread function). The arrows in Fig. 1 show the main structures common to all images.

HRA infrared images present some similarities with the large scale aspect of the nebula described by Cohen et al. (1975) at visible wavelengths : a North-South extension of the nebula (position angle (PA) roughly  $15^\circ$  to the East, slightly more than the value of  $7^\circ$  observed on a larger scale), a small bright inner quasi-rectangular core close to the star, and four prominent bright spikes emanating from its corners. Moreover, the increased angular resolution provided by speckle imaging and

adaptive optics, coupled with the fact that the optical depth is lower in the infrared than in the visible domain, reveal some small scale structures near the center of the nebula. For example, a structure extending up to about 0.5 arcsec from the central star is seen in the western direction (Fig. 1). This feature may result from the external edge of a possible accretion disc around HD 44179 (Roddier et al. 1995) or from some important ejection of matter produced by the presence of an hypothetical companion (Rouan 1993).

The hypothesis that bipolar nebulae are created from binary star systems by tidal interaction between a secondary and the expanding red giant primary was first proposed by Morris (1981). Cohen et al. (1975) as well as Greenstein and Oke (1977) and Rowan-Robinson and Harris (1983) suggest that a highly luminous companion, hidden in the dust, might explain the broad band spectrum of the source. However, as we show below by modelling the radiative transfer, the radiation from a single star, propagating through a non-spherical shell, also explains the broad band spectrum characteristics. The binary theory is supported by recent adaptive optics observations of Roddier et al. (1995) and by speckle observations of Meaburn et al. (1983), Leinert and Haas (1989) and Heintz (1990). It is important to notice that, since the first visual measurements in 1915, it is impossible to understand all of these measurements in terms of the orbital motion of two sources. However, very recent spectral measurements of Van Winckel et al. (1995) tend to give evidence for the binary nature of HD 44179. An orbital period of 298 days and a distance at periastron of about 0.50 AU (0.5 milliarcsec at 330 pc of distance according to Cohen et al. 1975) are estimated, much less than what has been proposed before ! Visual and speckle observations gave previously an angular separation of roughly 0.1 arcsec.

### 3. Observational constraints used for the Red Rectangle modelling

Four sets of data are considered:

a) Fig. 5c contains the existing spectrophotometric measurements from 0.13 $\mu$ m to 1300 $\mu$ m. The continuum displays a double bump shape that may be explained by different regimes in the radiative transfer (Lopez et al. 1995). Following this interpretation, the light scattered by dust particles is the main contributor for wavelengths below 1 $\mu$ m, while the thermal radiation from dust dominates above 1 $\mu$ m. It can be noticed that the double bump shaped spectrum of the Red Rectangle has some analogies with the spectrum of CRL 2688 (Ney et al. 1975), another post-AGB source.

b) The images on the photographic plates obtained by Cohen et al. (1975) are wavelength dependent. In red light, the nebula from which the Red Rectangle's nickname is derived, is characterized by a rectangular shape, an important extension on the sky (nearly one arcminute in size) and the presence of spikes. In other spectral bands of the visible domain, the appearance of the nebula is not so spectacular. However the rectangular shape of the nebula remains while less extended.

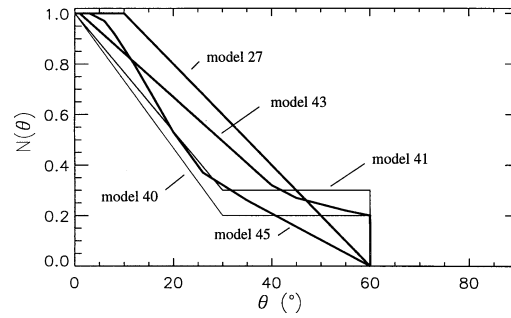


**Fig. 2.** Density laws used for models with an unique size of dust grain. The laws which give the best results are drawn with a thick line.

The images on the red photographic plates of the nebula seem to depend on some peculiar molecular emission still not well understood. The broad bump in the spectrum of the nebula analyzed by Schmidt et al. (1980) is superimposed with comparable intensity on the scattered stellar spectrum.

We can not yet reproduce, by a radiative transfer simulation, the extended red emission of the spectrum at visible wavelengths mentioned in our introduction. In the following, our goal has been limited to the modelling of the transfer of the light through the dust in the envelope when assuming that amorphous carbon is the only component of the dust.

c) The northern nebulosity has been observed by Schmidt et al. (1980) through a 2.8 arcsec circular aperture centered 10 arcsec north to the star. The continuum of the northern lobe spectrum measured in this diaphragm is about 1300 times lower than the stellar continuum. This ratio will be compared with what can be obtained by modelling.

d) The infrared images present some similarities with the aspects of the nebula at visible wavelengths. They are North-South elongated and display a rectangular shape with some East-West features not present in this case in the images obtained at visible wavelengths. In what follows, we have determined our model parameters by simulating infrared images at 2.2 $\mu$ m that we have compared visually with the elongated shape of the nebula. The western structure which appears in the infrared images is not taken into account in our model comparison. This structure might be real and caused by a concentration of dust.

### 4. The radiative transfer code

The problem of radiative transfer and radiative equilibrium is solved by a numerical simulation which is based on a Monte Carlo method. This method was often used in the case of spherical geometry (see for example Lefèvre et al. 1982). Details about the numerical simulation applied to axisymmetric dust nebulae are given by Lopez et al. (1995).

The numerical simulation aims at solving the problem of the radiative transfer through the dust shell and at computing the radiative equilibrium of dust grains. The star is assumed to radiate as a blackbody and is characterized by its effective temperature  $T_*$ . The spatial dust grains distribution is an axisymmetric function  $n(r, \theta)$ ,  $\theta$  being the latitude angle from the

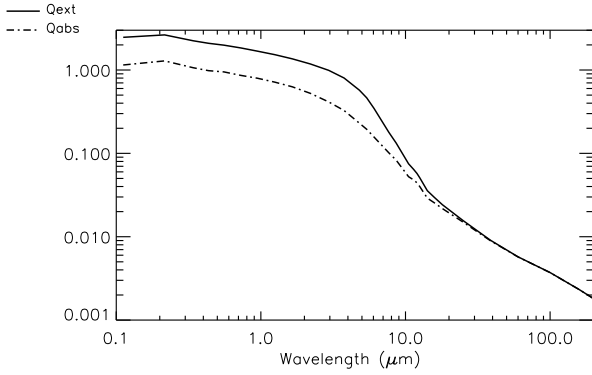


**Fig. 3.** Mean optical properties for a size distribution of amorphous carbon grains ( $0.05 \leq a \leq 1.2 \mu\text{m}$ ;  $dn \propto a^{-3} da$ ).

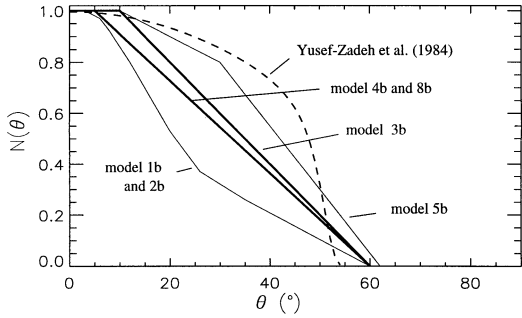


**Fig. 4.** Density laws used for models with a grain size distribution. The thick lines denote reasonably good models (model 3b, 4b and 8b). Over this range of function, our modelling becomes not satisfactory.

plane of the disc and  $r$  the radial distance from the center of the star given in photospheric radius units. The function  $n(r, \theta)$  is bounded by an inner and outer limits denoted  $R_{int}$  and  $R_{out}$  respectively. The dust grains are assumed to be of homogeneous composition and spherical with radius  $a$ . The Mie theory is used to calculate the optical constants of dust particles:  $Q_{ext}$  (the extinction efficiency),  $Q_{abs}$  (the absorption efficiency),  $Q_{sca}$  (the scattering efficiency) and  $S(\theta)$  (the scattering diagram) giving the angular dependence of the scattered radiation. Dust particles are supposed to be composed of amorphous carbon. The optical properties used come from Rouleau and Martin (1991). Although the PAH features are important for some of the nebula properties (see for example the infrared maps given by Bregman et al. 1993), the PAH molecules are not taken in account in the simulation.

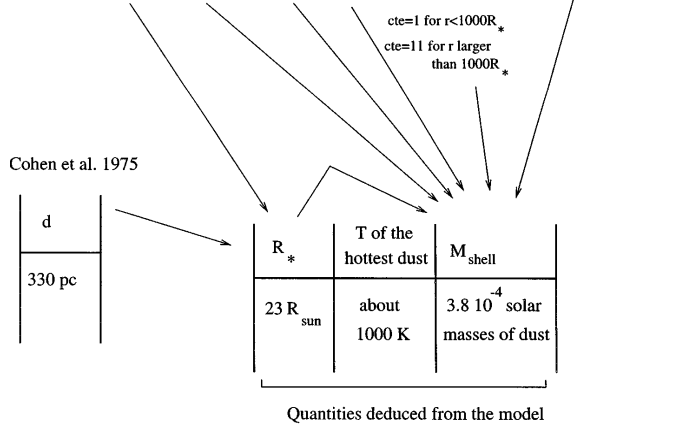
Along a radial direction, the spatial dust grains distribution function is related to the optical depth  $\tau_{ext}$  by:

$$\tau_{ext}(\lambda, \theta) = \int_{R_{int}}^{R_{out}} n(r, \theta) \pi a^2 Q_{ext}(\lambda) dr \quad (1)$$

According to the Monte Carlo method, stellar radiations and the thermal emission from dust particles are generated by a set of radiation trajectories. Thirty wavelengths are used to represent the emergent spectrum from the star and the emergent spectrum from dust particles.

**Table 1.** Red Rectangle model parameters for model 8b.

Model parameters						
$T_{eff}$	$\alpha_*$	$R_{int}$	$R_{ext}$	a grains	$n(r, \theta)$	$\tau_{ext}(\lambda=1\mu\text{m}, \theta=0^\circ)$
7500 K	0.33 mas	$55 R_*$ $\pm 5 R_*$	$90000 R_*$	from 0.05 to 1.2 $\mu\text{m}$	$k.cte.N(\theta).r^{-2}$ $k=4.16 \cdot 10^{-23} d$	$9.5 \pm 1$



At the beginning of the algorithm, radiations are first emitted by the star. The direction of initial propagation of one radiation is chosen randomly. The length  $l$  of the effective radiation trajectory from the origin of emission up to the interaction with a grain of the dusty envelope is chosen randomly. The density probability of the random process is proportional to  $\exp(-\tau)$ , where  $\tau$  is the optical depth along the direction of propagation. For each interaction, a fraction of the radiation leaves the envelope, a fraction is absorbed and a fraction is scattered. The direction of scattering is randomly chosen according to the scattering diagram  $S(\theta)$ . The scattered fraction of the radiation continues then to propagate in the three dimensional dusty medium. Several interactions with dust grains will successively occur. Each time the energy of the scattered radiation becomes lower. After most of its initial energy is lost from multiple scattering, the propagating radiation is neglected. New radiations are then generated from the star and later in the process from thermally emitting dust particles.

The radiative equilibrium of the dust particle which depends on both the stellar radiation and the grain-grain radiative exchanges is determined in a self consistent way. In the present simulation the dust shell is sampled in about 400 tori in each of which the grain temperature is constant for axisymmetry reasons. Radiative exchanges between the star and tori and between each torus and other tori constrain the radiative equilibrium relation. This relation which equates in each torus the total amount of absorbed energy to the total amount of emitted energy provides the temperature of the dust.

The brightness distribution of the object (as a function of wavelength and inclination angle of the nebula) as well as its broad band spectrum (depending also on inclination angle of the nebula) are obtained for a given set of parameters characterizing the model. A solution for the parameters is searched empirically

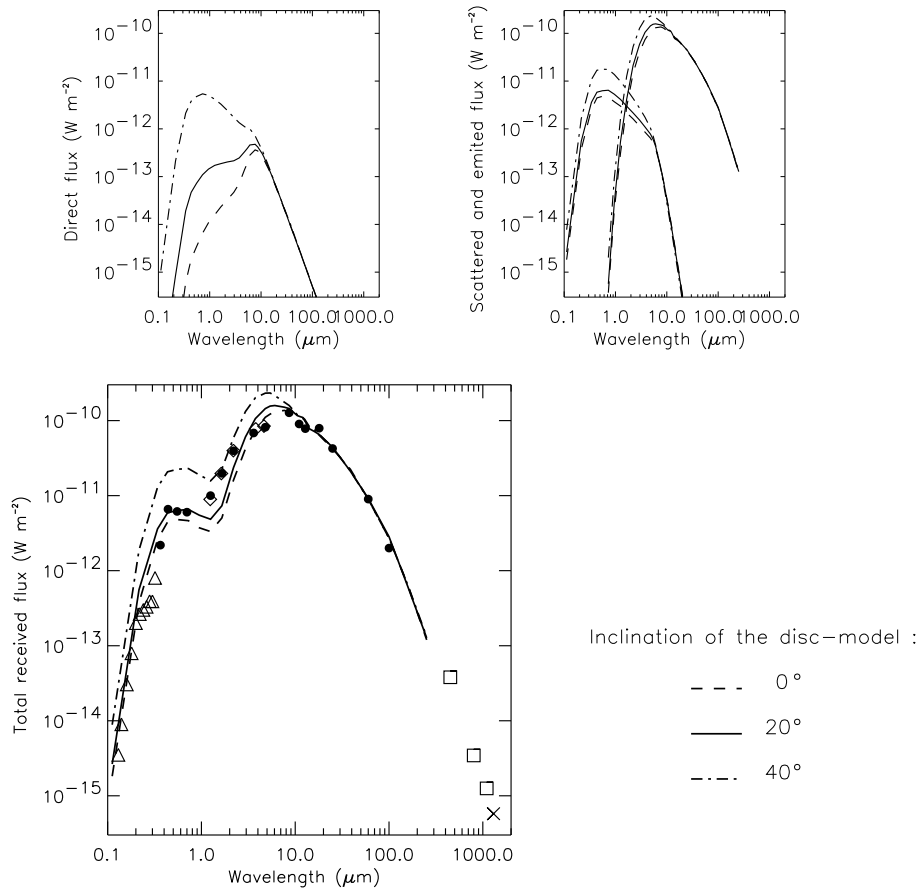


**Fig. 5.** The spectrum of the Red Rectangle compared to what is obtained from modelling (model 8b) for different view angles. Different sets of data are displayed: ● photometric compilation of Leinert and Haas (1989), △ sample of the UV-spectrometric measurement of Sitko (1981), ◇ our IR photometric measurements (ESO 1-m telescope, Dec. 24/25 1988), □ submillimeter measurements of van der Veen et al. (1994) and × the 1.3 mm measurement of Walmsley et al. (1991).

until the results of the simulation reproduce the existing measurements.

## 5. The models

Two kinds of model have been processed. The grain size is assumed to be unique at first while a distribution of grain dimensions is considered subsequently.

### 5.1. Results and validity for the unique grain size modelling

In a first approach a model of the Red Rectangle has been proposed by Lopez et al. (1995). It reproduces the appearance of the nebula at visible wavelengths and its broad band spectrum. We try now, by varying the model parameters in a wider range, to explain also the infrared shape of the nebula (North/South extension).

The spatial distribution of the dust density is a function of the radial distance,  $r$ , and of the latitude angle,  $\theta$ . We have separated the variables according to:

$$n(r, \theta) \propto N(\theta)r^{-\alpha}. \quad (2)$$

The results of the simulation show that the observational constraints considered, i.e. the broad band spectrum and the elongated shape of the nebula at visible and near infrared wavelengths, cannot be satisfied with a unique set of model param-

eters. The following choice, for the model parameters, is the best compromise:

- The functions  $N(\theta)$  giving good results are displayed in Fig. 2.
- The stellar temperature of the models is set to 7500 K.
- The angular radius of the star is  $0.33 \times 10^{-3}$  arcsec. Once the shape of the emergent spectrum is reproduced, this angular radius results from the fit of the bolometric flux of our model to the received bolometric flux.
- $R_{int}$  ranges from 100 to 250 stellar radii.  $R_{ext}$  is not a sensitive parameter and has been set to about  $10^5$  stellar radii in order to be consistent with the angular dimension of the nebula at visible wavelengths.
- The exponent  $\alpha$  of the dust density law of Eq. 2 is not a very sensitive parameter and has been set to unity for  $r > 250$  stellar radii. Putting more dust (by modifying the radial dependence of the density law) between 100 and 250 stellar radii strongly improves the quality of the fit of the spectrum in the near infrared range.
- The optical depth in the equatorial plane of the disc,  $\tau_{ext}(\lambda = 1\mu\text{m}, \theta = 0^\circ)$ , ranges from 10 to 14.
- The dust grain radius reproducing best the spectrum and the shape at visible wavelengths is about  $0.25\mu\text{m}$ . Dust grain size must be increased up to at least  $0.5\mu\text{m}$  in order to reproduce the North/South extension of the  $2.2\mu\text{m}$  infrared image.

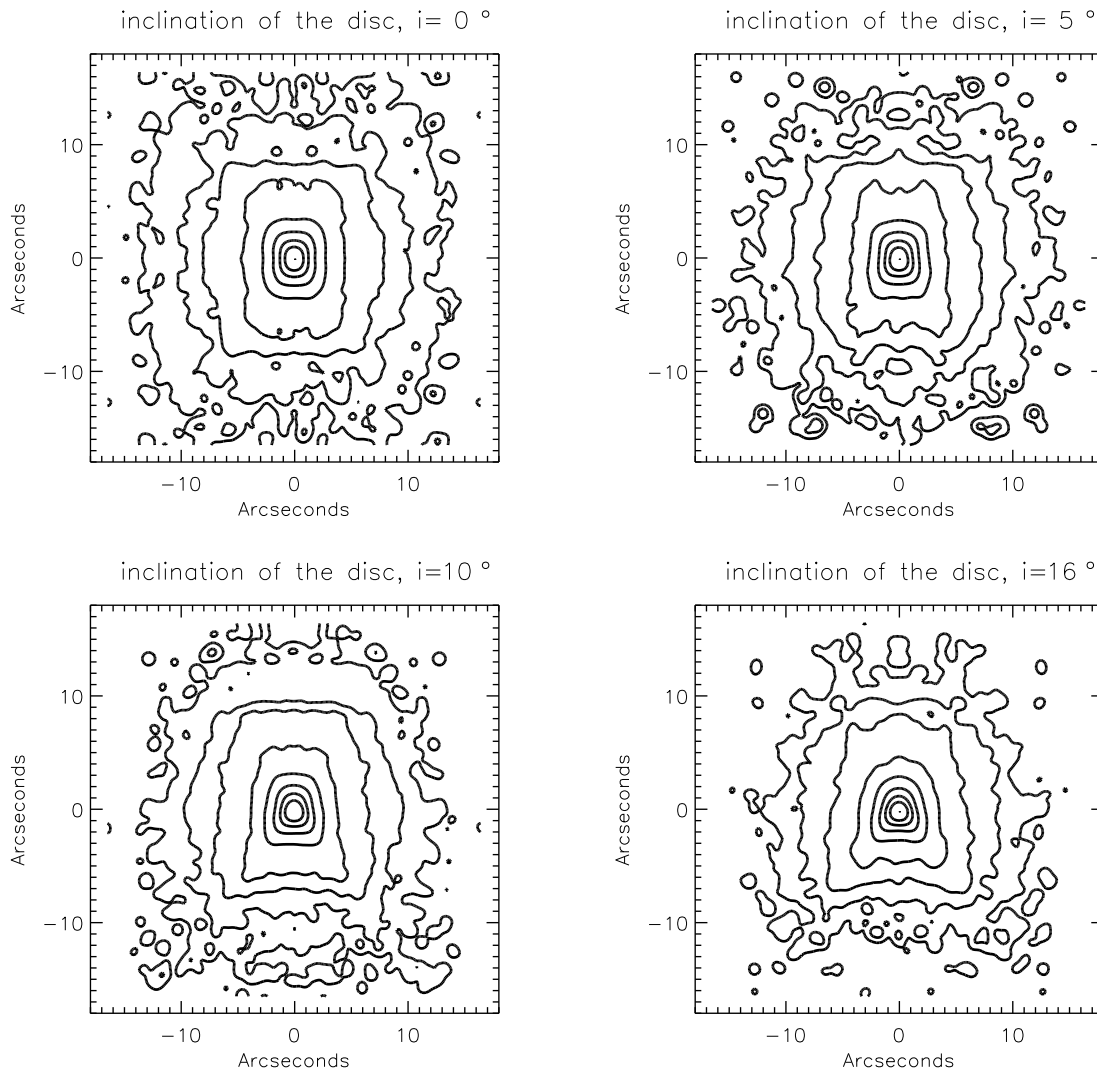


**Fig. 6.** Images simulated at  $0.5 \mu\text{m}$  for different view angles (model 8b). Each image is convolved by a Gaussian with  $\sigma = 0.4$  arcsec. The ratio between two successive contour levels is 3.2.

### 5.2. Modelling with a grain size distribution

The scattering by particles with a radius of at least  $0.5 \mu\text{m}$  is a necessary condition to produce the extended shape of the nebula at  $2.2 \mu\text{m}$ . The following grain size distribution used in our new model is :

$$dn \propto a^{-\beta} da \quad (3)$$

where  $a$  is the radius of the grain. Ideally, the computation of radiative transfer by a Monte Carlo method requires a random choice of the size of the grain interacting with the radiation field. However, we decided for practical reasons to average the optical grain properties over the different sizes and to create a kind of hybrid grain (Fig. 3). The use of a hybrid grain leads to a mean value for the temperature although the equilibrium temperatures of grains of different sizes located at the same distance from the star are different.

The mean section of the dust particles is given by,

$$\langle s \rangle = \pi a_{rms}^2 \quad (4)$$

with,

$$a_{rms} = \left( \int_{a_{min}}^{a_{max}} a^{-\beta+2} da / \int_{a_{min}}^{a_{max}} a^{-\beta} da \right)^{1/2} \quad (5)$$

Optical properties are averaged according to the following relations,

$$\langle Q_{abs}(a, \lambda) \rangle = \frac{\int_{a_{min}}^{a_{max}} Q_{abs}(a, \lambda) a^{-\beta+2} da}{\int_{a_{min}}^{a_{max}} a^{-\beta+2} da} \quad (6)$$

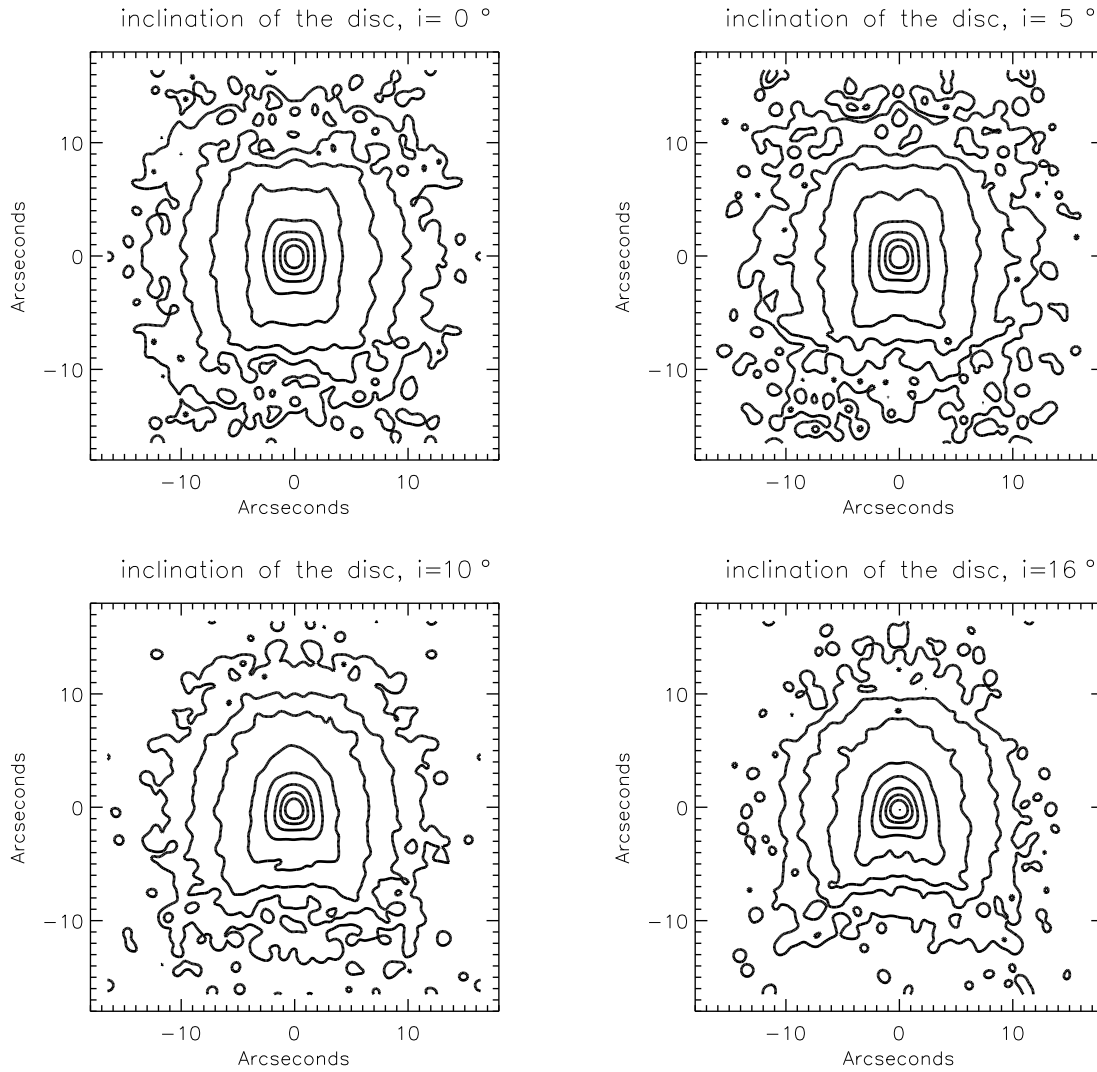


**Fig. 7.** Same than Fig. 6 at  $0.7 \mu\text{m}$  of wavelength.

$$\langle Q_{sca}(a, \lambda) \rangle = \frac{\int_{a_{min}}^{a_{max}} Q_{sca}(a, \lambda) a^{-\beta+2} da}{\int_{a_{min}}^{a_{max}} a^{-\beta+2} da} \quad (7)$$

where  $Q_{abs}$  and  $Q_{sca}$  are the optical efficiencies for absorption and scattering. The phase function  $S(\theta)$  is averaged over the cross section for scattering,  $\pi a^2 Q_{sca}$ ,

$$\langle S(\theta, a, \lambda) \rangle = \frac{\int_{a_{min}}^{a_{max}} S(\theta, a, \lambda) Q_{sca}(a, \lambda) a^{-\beta+2} da}{\int_{a_{min}}^{a_{max}} Q_{sca}(a, \lambda) a^{-\beta+2} da} \quad (8)$$

Many models have been tested. The best results have been obtained with the latitude functions  $N(\theta)$  displayed in Fig. 4. The following parameters have been obtained (see Table 1):

- $T_{eff} = 7500 \text{ K}$

- the angular radius of the star  $\alpha_* = 0.33 \times 10^{-3} \text{ arcsec}$  (consistent with the amount of the received bolometric flux)

- $R_{int} = 55 \pm 5 R_*$ ;  $R_{ext} = 90000 R_*$

- $n(r, \theta) \propto N(\theta) \times r^{-2}$ . When  $r > 1000 R_*$ , the density law  $n(r, \theta)$  must be multiplied by 11 (see Table 1) to fit the near infrared spectrum. The radial dependency of the density does not seem to be a pure power function.  $R_{int}$  and  $n(r, \theta)$  near the star ( $r < 1000 R_*$ ) are parameters that cannot be separately determined because of the limited angular resolution of the infrared images used as constraints for the model.

- $\tau_{ext}(\lambda = 1 \mu\text{m}, \theta = 0^\circ) = 9.5$  in the plane of the disc. In a slightly different model, it could be increased up to 11.

- $0.05 \mu\text{m} < a < 1.2 \mu\text{m}$  with a size distribution in  $a^{-3}$ .

With this set of parameters:

- a good fit to the emergent spectrum (see Fig. 5) is obtained from 0.13 to about  $250 \mu\text{m}$  ( $250 \mu\text{m}$  being the maximum wavelength for which the radiative transfer is here simulated).

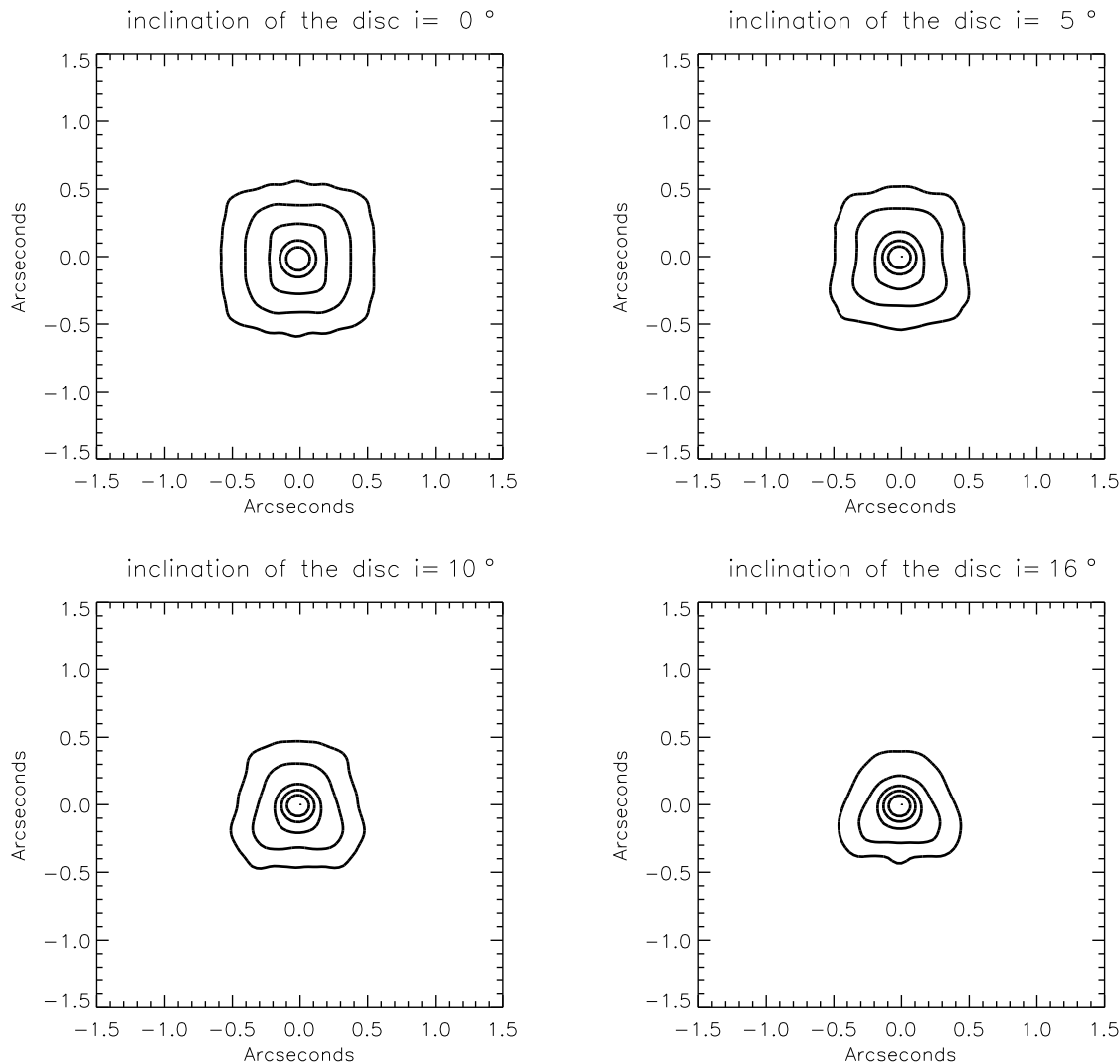


**Fig. 8.** Images simulated at  $2.2 \mu\text{m}$  (model 8b). Each image is convolved by a Gaussian with  $\sigma = 0.05$  arcsec. The ratio between two successive contour levels is 2.2. The image field is smaller than at visible wavelength.

- The images simulated at  $0.5$  and  $0.7 \mu\text{m}$  are shown in Figs. 6 and 7 for different inclinations of the plane of the disc with respect to the line of sight. The rectangular aspect holds for an inclination angle less than  $10^\circ$ .

- The observations of Schmidt et al. (1980) give a ratio of 1300 between the flux measured through a  $2.8$  arcsec aperture at the center of the nebula and the flux measured at  $10$  arcsec distance in the northern lobe. At  $0.7 \mu\text{m}$ , our model gives a value of this ratio of the order of 2000 for inclinations less than  $10^\circ$ .

- the images simulated at  $2.2 \mu\text{m}$  have a square shape (see Fig. 7).

These results are reasonably good, except that the near infrared image of the model is still not as elongated as observed. Increasing more the size of the dust grains does not have much effect, while increasing the optical depth does. Varying  $\tau_{\text{ext}}(\lambda = 1 \mu\text{m}, \theta = 0^\circ)$  from 9.5 to 15 squeezes the nebula in the

plane of the disc as shown in Fig. 9. In this case, the fit to the other observational constraints, such as the spectrum, is lost.

## 6. Discussion

In spite of some limitations (e.g. difficulties in getting the near infrared shape of the nebula), the last model detailed above is coherent with a set of observational constraints characterizing the bipolar nebula. Our radiative transfer modelling is still valid if the central source is a binary star, except if the luminosity of the companion cannot be neglected with respect to the main star and if their spectral types differ. In this case, the central source cannot be represented as a single blackbody.

One of the main results of our study is the estimation of the dust density law. While the model of Yusef-Zadeh et al. (1984) reproduces the aspect of the nebula at visible wavelengths, it does not allow to fit the broad band spectrum. Our density laws  $N(\theta)$  (Fig. 4) decrease more rapidly for the first few tens of

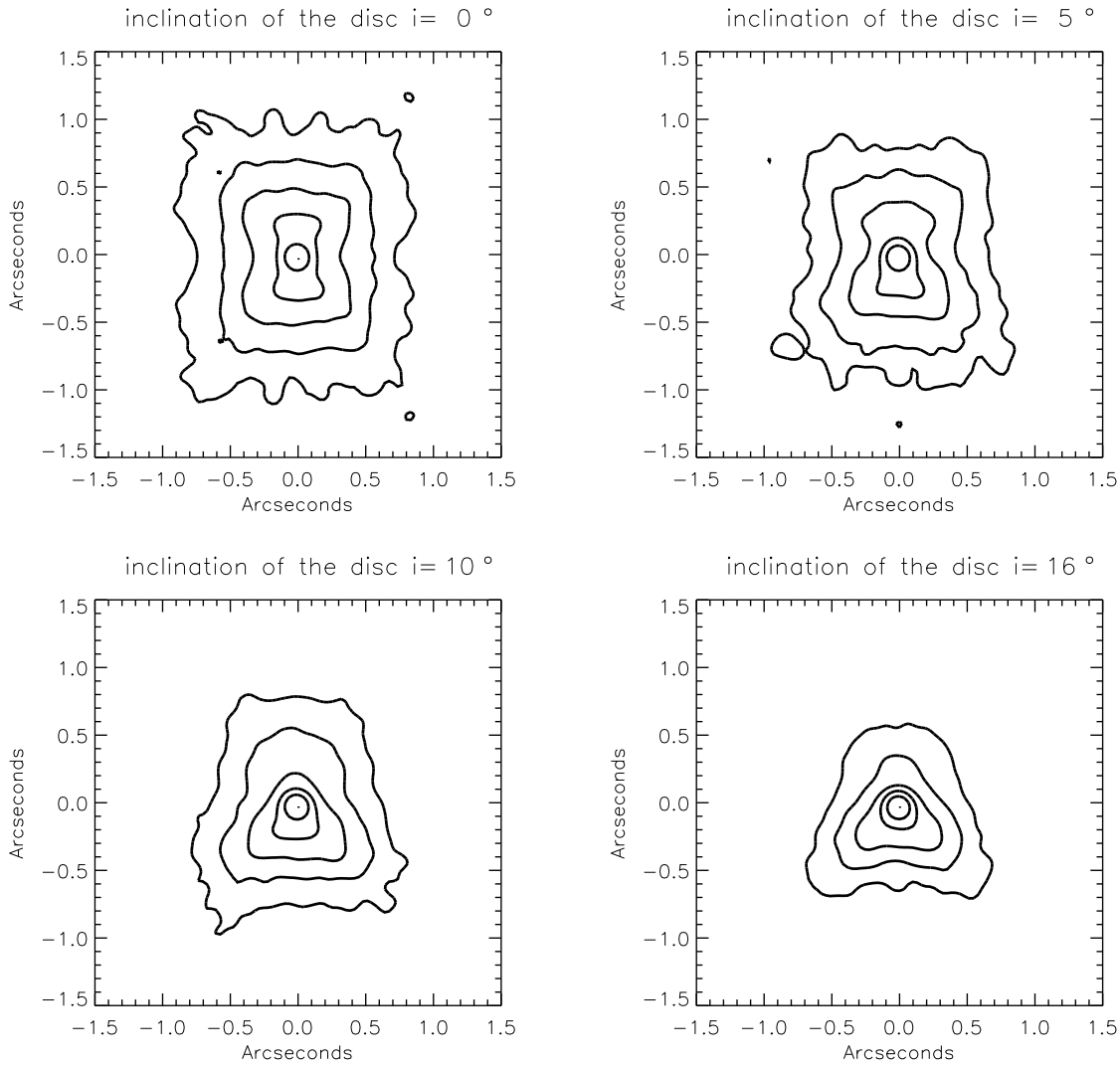


**Fig. 9.** Same than Fig. 8. The optical depth,  $\tau_{ext}(\lambda = 1\mu\text{m})$  has been increased from 9.5 (model 8b) up to 15.

degrees above (and below) the plane of the disc than the density law of Yusef-Zadeh et al.

The temperature of the hottest dust grains (located near the star) is found to be 1010 K. The number of dust particles in the equatorial plane and at the inner limit of the disc is  $n \simeq 170 \text{ grains/m}^3$ , assuming that the Red Rectangle is located at  $d = 330 \text{ pc}$  (Cohen et al. 1975) and according to the following relation based on our modelling (model 8b) :

$$n(r = 55R_*, \theta = 0^\circ) = 5.7 \cdot 10^4 \times d^{-1} \text{ grains.m}^{-3} \quad (9)$$

If we take  $\rho = 2.2 \cdot 10^3 \text{ kg m}^{-3}$  for the mass density of the dust grains, the mass of grains contained in the shell is :

$$M_{shell} = 3.5 \cdot 10^{-9} d^2 M_\odot \quad (10)$$

With  $d = 330 \text{ pc}$ ,  $M_{shell}$  is about  $3.8 \cdot 10^{-4} M_\odot$  for model 8b ( $3.4 \cdot 10^{-4} M_\odot$  for model 3b). The accuracy of this mass determination depends on the accuracy on which, among other parameters,  $R_{ext}$  is derived. In our model,  $R_{ext} = 90000 R_*$

corresponds on the sky to nearly 30 arcsec. This is approximately the size of the angular extent of the reflexion nebosity (Fig. 1c of Cohen et al. 1975). If some dust located at larger distance and not detected in the images of Cohen et al. (1975) do exist, then the total dust mass value given above is a minimum. Assuming that the mass ratio of gas to dust is  $158 \pm 13$  (Knapp 1986), the total mass of the envelope of HD 44179 is estimated to be  $6.0 \cdot 10^{-2} M_\odot$  (model 8b). But this latter assumption is very uncertain (Jura, 1996) : we know that there has apparently been at least some separation of the gas and dust because the best way to explain the abundances in the photosphere of HD 44179 is that the star has accreted gas but not dust; the CO lines appear to be weak compared to the far infrared flux, consistent with a low gas to dust ratio.

Large particles are present in the circumstellar environment of HD 44179, a conclusion already drawn by Cohen et al. (1975) from optical polarimetric measurements. Our attempts made to reproduce the North/South elongated shape of the  $2.2\mu\text{m}$

infrared image show that particles of at least  $1.2\mu\text{m}$  in size are expected. From CO measurements of the envelope in the radio domain, Jura et al. (1995) show that particles as large as  $20\mu\text{m}$  might be found around the Red Rectangle, and, that much of the material is enclosed in a long-lived structure such as a gravitationally bound disc.

In our model, grains of different sizes are assumed to follow the same spatial distribution. However, larger particules probably concentrate in the equatorial plane because condensation and aggregation of dust should occur more efficiently in the plane of the disc where the density is high. For large particles, the expected  $N(\theta)$  may therefore have a sharper decrease than in Fig. 4. The difficulty to reproduce with our model the  $2.2\mu\text{m}$  North/South extension suggests that such a spatial distribution, function of the size of the particles, must be considered.

Our assumption that the decrease of the dust density with regards to the radial distance is independent of the latitude angle  $\theta$ , may be far from reality. An alternative assumption has been proposed by Icke (1981) who suggested that the radial expansion of bipolar nebulae might depend on the latitude angle. In the case of HD 44179, a small and optically thick torus of dust may produce the appearance of the nebula. This is compatible with the conclusion of Jura et al. (1995) on the existence of a long-lived disc. The western structure seen in our infrared compilation (Fig. 1) may be related to the spatial limits of this disc (Roddier et al. 1995).

The next step of this study will be to consider a disc limited in extension in our model. In parallel, more infrared observations with a better angular resolution are needed for understanding the nearby star environment of HD 44179 and for confirming or not the presence of this disc.

*Acknowledgements.* We are grateful to Daniel Rouan for useful discussions and to our referee Mike Jura for his comments. We also thank John Tully and Djamel Mékarnia for their reading of the manuscript.

## References

- Allamandola, L.J., 1989, in UAI symposium 135 :“Interstellar Dust”, eds. Allamandola, L.J., and Tiellens, A.G.G.M. (Dordrech: Kluwer), p.129
- Bachiller, R., Gómez-González, J., Bujarrabal, V., Martín-Pintado, J., 1988, A&A 196, L5
- Bregman, J.D., Rank, D., Temi, P., Hudgins, D., Kay, L., 1993, ApJ 411, 794
- Cohen, M., Anderson, C.M., Cowley, A., et al., 1975, ApJ 196, 179
- Cruzalèbes, P., Tessier, E., Lopez, B., Eckart, A., 1996, A&AS 116, 597
- Duley, W.W., 1985, MNRAS 215, 259
- Duley, W.W., Williams, D.A., 1981, MNRAS 196, 269
- Greenstein, J.L., Oke, J.B., 1977, PASP 89, 131
- Heintz, W.D., 1990, MNRAS 245, 759
- Icke, V., 1981, ApJ 247, 152
- Jura, M., Balm, S.P., Kahane, C., 1995, ApJ 453, 721J
- Knapp, G.R., 1986, ApJ 311, 731
- Lefèvre, J., Bergeat, J., Daniel, J.Y., 1982, A&A 114, 341
- Leinert, Ch., Haas, M., 1989, A&A 221, 110
- Léger, A., Puget, J.-L., 1984, A&A 137, L5
- Lopez, B., Mékarnia, D., Lefèvre, J., 1995, A&A 296, 752
- Mathis, J.S., Lamers, H.J.G.L.M., 1992, A&A 259, L39
- Meaburn, J., Walsh, J.R., Hebden, J.C., Moragn, B.L., Vine, H., 1983, MNRAS 205, 53P
- Morris, M., 1981, ApJ 249,572
- Ney, E.P., Merrill, K.M., Becklin, E.E., Neugebauer, G., Wynn-Williams, C.G., 1975, ApJ 198, L129
- Perkins, M.G., Scarrot, S.M., Murdin, P., Bingham, R.G., 1981, MNRAS 196, 635
- Roddier, F., Roddier, C., Graves, J.E., Northcott, M.J., 1995, ApJ 443, 249
- Rouan, D., 1993, Sub-arcsec IR imaging of Transition Objects, in : “proceedings of the ESO/CTIO workshop Mass loss on the AGB and beyond” La Serena, jan 1992, Schwarz Ed.
- Rouleau, F., Martin, P.G., 1991, ApJ 377, 526
- Rowan-Robinson, M., Harris, S., 1983, MNRAS 202, 767
- Sakata, A., Wada, S., Tanabe, T., Onaka, T., 1984, ApJ 287, L51
- Scarrott, S.M., Watkin, S., Miles, J.R., Sarre, P.J., 1992, MNRAS 255, 11p
- Schmidt, G.D., Witt, A.N., 1991 ApJ 383, 698
- Schmidt, G.D., Cohen, M., Margon, B., 1980, ApJ 239, L133
- Sitko, M. L., 1983, ApJ 265, 848
- Tessier, E., Perrier, C., Léna, P., Michel, G., Langlet, A., 1990, Diffraction-limited imaging of the Red Rectangle and R Aquarii in the L Band, in: “Astrophysics with infrared arrays”, ASP Conference Series, Vol. 14, Richard Elston Ed.
- van der Veen, W.E.C.J., Waters, L.B.F.M., Trams, N.R., Matthews, H.E., 1994, A&A 285, 551
- Van Winckel, H., Waelkens, C., Waters, L.B.F.M., 1995, A&A 293, L25
- Waelkens, C., Van Winckel, H., Trams, N.R., Waters, L.B.F.M., 1992, A&A 256, L15
- Walmsley, C.M., Chini, R., Kreysa, E., Steppe, H., Forveille, T., Omont, A., 1991, A&A 248, 555
- Waters, L.B.F.M., Trams, N.R., Waelkens, C., 1992, A&A 262, L37
- Yusef-Zadeh, F., Morris, M., White, R., 1984, ApJ 278, 186